Auroral electron distributions derived from combined UV and X-ray emissions

N. Østgaard,[1,2] J. Stadsnes,[3] J. Bjordal,[3,4] G. A. Germany,[5] R. R.Vondrak,[6] G. K. Parks,[7] S. A. Cummer,[8] D. L. Chenette,[9] and J. G. Pronko[10]

Abstract. The Polar Ionospheric X-ray Imaging Experiment and the Ultraviolet Imager on board the Polar satellite provide the first simultaneous global scale views of the electron precipitation over a wide range of electron energies. By combining the results from these two remote sensing techniques we have developed a method to derive the electron energy distributions that reproduce the true electron spectra from 1 to 100 keV and that can be used to calculate the energy flux in the energy range from 100 eV to 100 keV. The electron energy spectra obtained by remote sensing techniques in three 5-min time intervals on July 9 and July 31, 1997, are compared with the spectra measured by low-altitude satellites in the conjugate hemisphere. In the energy range from 90 eV to 30 keV the derived energy flux is found to be 1.03±0.6 of the measured energy fluxes. The method enables us to present 5-min time-averaged global maps of precipitating electron energy fluxes with a spatial resolution of ∼700 km. The study shows that the combination of UV and X-ray cameras on a polar orbiting spacecraft enables comprehensive monitoring of the global energy deposition from precipitating electrons over the energy range that is most important for magnetosphere-ionosphere coupling.

1. Introduction

Remote sensing by imagers designed to measure auroral emissions at different wavelengths provides global information about how the electron precipitation varies spatially and temporally. By utilizing appropriate techniques it is possible to derive the electron energy distribution and hence examine the energy input to the ionosphere [*Robinson and Vondrak*, 1994]. To explore and to utilize these tools and techniques, the Polar spacecraft was equipped with imagers to measure the aurora in three different wavelength regions, that is, the visible emissions, the ultraviolet (UV) emissions and X rays [*Acuña et al.*, 1995].

From measurements of visible and UV emissions it has been found that the ratio of intensities from different emissions lines or bands can be used to estimate the average electron energy [*Eather and Mende*, 1971; *Rees and Luckey*, 1974; *Strickland and Anderson*, 1983; *Steele and McEwen*, 1990]. Together with a line or a band of emissions that is proportional to the total electron energy flux, a two-parameter electron distribution can be derived. Such a technique was used by *Germany et al.* [1997, 1998a, 1998b] to derive electron energy fluxes and average electron energies from the Ultraviolet Imager (UVI) [*Torr et al.*, 1995] measurements, and their results were found to agree fairly well with the simultaneous electron measurements from the Defense Meteorological Satellite Program (DMSP) spacecraft. As the production of X-ray bremsstrahlung is fairly well

[1]Department of Physics, University of Oslo, Oslo, Norway
[2]Now at Laboratory for Extraterrestrial Physics, Goddard Space Flight Center, Greenbelt, Maryland, USA
[3]Department of Physics, University of Bergen, Bergen, Norway
[4]Deceased July 17, 2001
[5]The Center for Space Plasma, Aeronomy, and Astrophysics Research, University of Alabama, Huntsville, Alabama, USA.
[6]Laboratory for Extraterrestrial Physics, Goddard Space Flight Center, Greenbelt, Maryland, USA.
[7]Geophysics Program, University of Washington, Seattle, Washington, USA.
[8]Electrical and Computer Engineering Department, Duke University, Durham, North Carolina, USA.
[9] Lockheed-Martin Advanced Technology Center, Palo Alto, California, USA.
[10] Physics Department, University of Nevada, Reno, Nevada, USA.

understood, the X-ray production from electron precipitation can be estimated and several deconvolution techniques has been developed over the last decades [*Rees*, 1964; *Kamiyama*, 1966; *Berger et al.*, 1970; *Berger and Seltzer*, 1972; *Seltzer and Berger*, 1974; *Luhmann and Blake*, 1977; *Walt et al.*, 1979; *Khosa et al.*, 1984; *Robinson et al.*, 1989; *Gorney*, 1987; *Lorence*, 1992]. *Anderson et al.* [1998] and *Østgaard et al.* [2000] utilized such techniques and showed that the X-ray measurements by the Polar Ionospheric X-ray Imaging Experiment (PIXIE) [*Imhof et al.*, 1995] can be used to derive the auroral electron energy spectrum above ∼3 keV. Comparing the derived electron spectra with the measured electron energy fluxes by DMSP, they both found a fairly good agreement in the electron energy range from 3 to 30 keV. As *Østgaard et al.* [2000] also utilized the high-energy X rays (∼8 - 22 keV) from PIXIE they were able to capture the frequently observed energetic tail (>20 - 30 keV up to ∼100 keV) of the auroral electron spectrum [*Miller and Vondrak*, 1985] which can contribute substantially to the total energy flux.

In this study we report how the combined measurements from these two imagers, PIXIE and UVI, can be used to obtain the electron energy flux from 100 eV to 100 keV as well as the shape of the electron spectra from 1 to 100 keV, and consequently monitor the electron distribution over the energy range that is important for magnetosphere-ionosphere (MI) coupling. The imaging results are evaluated by comparing the energy spectra obtained from the remote sensing techniques with the electron spectra measured by the DMSP spacecraft passing through the auroral region at ∼800 km altitude in the conjugate hemisphere. To present the technique, we have chosen three 5-min time frames from two substorms that occurred on July 9 and July 31, 1997, when the Polar satellite was at apogee (∼8.5 R_E), well located for both imagers to measure the entire auroral oval in the Northern Hemisphere. The July 31 substorm has been examined by *Østgaard et al.* [2000]. We show that the technique enables us to generate 5-min time-averaged global maps of precipitating electron energy fluxes with a spatial resolution of ∼700 km. As the method not only gives us the total energy flux from 100 eV to 100 keV but also the shape of the electron spectra above 1 keV, the energy flux can be calculated in different energy ranges, for example, above and below 10 keV. Although the derivation techniques based on UV and X-ray measurements are not new, the combined use of UV and X rays enables us to derive the electron energy distribution over a wider energy range that none of the imagers can provide alone. This has not been shown before and represents a new tool for auroral research.

2. Deriving Electron Spectra From PIXIE and UVI

In Plate 1 we show two time frames of the UV and X-ray images from July 31, 1997. The arrows in the middle panels indicate the DMSP trajectories during the 5 min used to accumulate X rays, traced along the magnetic field to get the conjugate magnetic trajectories in the Northern Hemisphere. The red boxes in the middle panels indicate the spatial resolution used to derive the electron energy distribution.

As the technique of deriving a four-parameter electron distribution from the PIXIE measurements is discussed elsewhere [*Østgaard et al.*, 2000], we only give a brief description here. PIXIE is a pinhole camera measuring X rays from ∼3 to 22 keV. As each X-ray photon is tagged with energy, time, and location, the time and space resolutions are adjustable depending on the strength of the event. A detailed description of the data processing from PIXIE is given by *Østgaard et al.* [1999]. For this study we have also performed an analysis of the gain shift across the focal plane of the detector that was not included in the paper by *Østgaard et al.* [2000], which slightly affects the energy determination of the X rays. The bremsstrahlung production efficiency increases with increasing electron energies, but for electrons with typical energies in auroras, the X-ray production rate is very small. X-ray measurements often suffer from poor statistics when spectral information is extracted. To overcome this problem we bin the X rays in the original 63 low-energy channels into four energy bands, and we bin the X rays in 12 of the original high-energy channels into two energy bands. The lower threshold of spatial resolution is determined by the pinhole size. At 6-8 R_E the projected size of the pinhole corresponds to ∼600-900 km in the ionosphere. At this radial distance the wobbling of the despun platform smears out the image by 210-290 km in one dimension and the 5 min accumulation time needed to get sufficient count rates of X rays in all energy bands introduces a smearing of ∼100 km along the trajectory of the satellites foot point. When integrating the X rays we have used regions of 6° latitude in corrected geomagnetic coordinates (CGM) and 1-hour magnetic local time (MLT) sector as indicated by the red boxes in Plate 1b. These boxes correspond to a 670 km × 670 km region in the ionosphere (100 km altitude) at 66° CGM latitude, increasing (decreasing) to a 960 (320) km ×

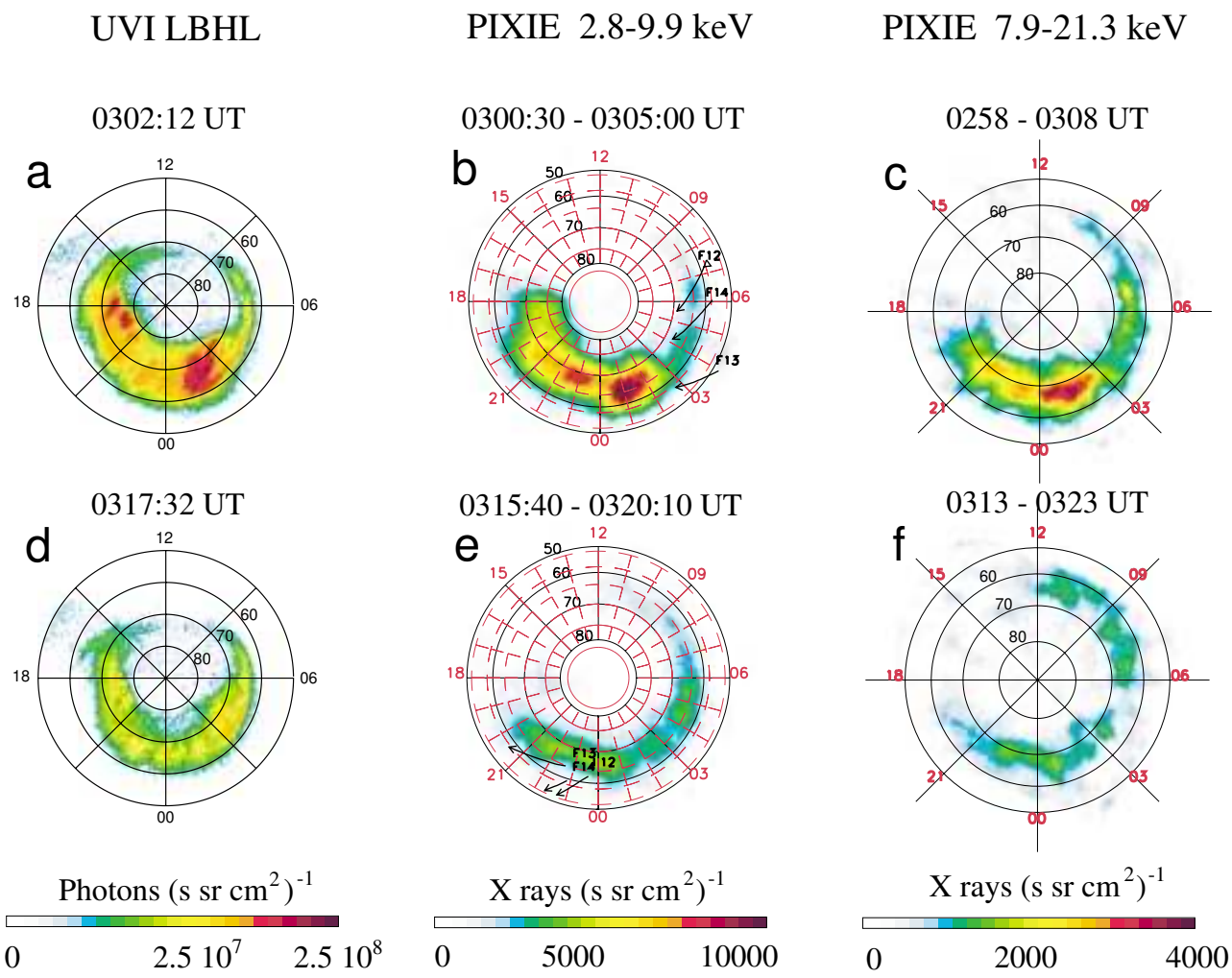

Plate 1. Global images of UV and X-ray emissions at two different times on July 31, 1997. (a, d) UVI LBHL images; 36.8 s time exposure; dayglow is removed. (b, e) PIXIE (2.8-9.9 keV) images accumulated for 5 min. Trajectories of the DMSP spacecraft during the 5 min accumulation time are shown by arrows. The spatial resolution used for deriving electron energy spectra are shown by dashed red lines. (c, f) PIXIE (7.9-21.3 keV) images accumulated for 10 min. The four PIXIE images in Plates 1b, 1c, 1e and 1f were also shown by *Østgaard et al.* [2000].

670 km at 55° (79°) CGM latitude, which is the lowest (highest) center latitude of the boxes we use. Throughout the text we will refer to these boxes as ∼700-km boxes, although their size varies with latitude. For detailed comparison with in situ measurements, the size of the integration area of X rays must be considered more carefully than these boxes provide. However, for this study we obtain the 5-min time average X-ray spectra along the auroral zone with a spatial resolution of ∼700 km. To derive the electron spectrum from the X-ray spectrum, we use a look-up table of the angular dependent X-ray spectra produced by single exponential electron spectra generated on the basis of the "general electron-photon transport code" of *Lorence* [1992]. This code takes into account the scattering of electrons, production of secondary electrons, angular dependent X-ray production, photoelectric absorption of X rays and Compton scattering of X rays. From the look-up table we find the single exponential electron spectrum that produces the best fit to the measured X-ray spectrum. As the measured X-ray spectrum often shows a hard tail, we also add the X-ray production from two exponential electron spectra to find a double exponential electron spectrum that may give a more accurate fit to the measured X-ray spectrum. A chi-square test is performed to find which of the single or double exponential electron spectra that produces the best fit to the measured X-ray spectrum. In Figure 1 we show four of the measured X-ray spectra together with the best fit of X-ray production from single or double exponential electron spectra.

The technique for using measurements from the UVI instrument as remote diagnostics is discussed by *Germany et al.* [1997, 1998a, 1998b], and we only describe the basic principles of the technique here. The UVI provides global images of emission within the Lyman-Birge-Hopfield (LBH) band (140 - 180 nm) which would ideally yield the total energy influx of electron precipitation above the excitation energy level (∼7 eV). However, the O_2 Schumann-Runge absorption continuum peaks at the shorter wavelengths within the UVI band pass and decreases with longer wavelengths. Due to improved filter techniques the UVI instrument is designed to provide separate measurements within the LBH band. One filter covers the short wavelength portion of the LBH band (LBHS 140 - 160) which is subject to significantly greater O_2 absorption relative to the longer wavelength range covered by the LBH long filter (LBHL: 160 - 180 nm). Electrons at higher energies deposit their energies at lower altitudes and the UV emissions produced deep down in the atmosphere

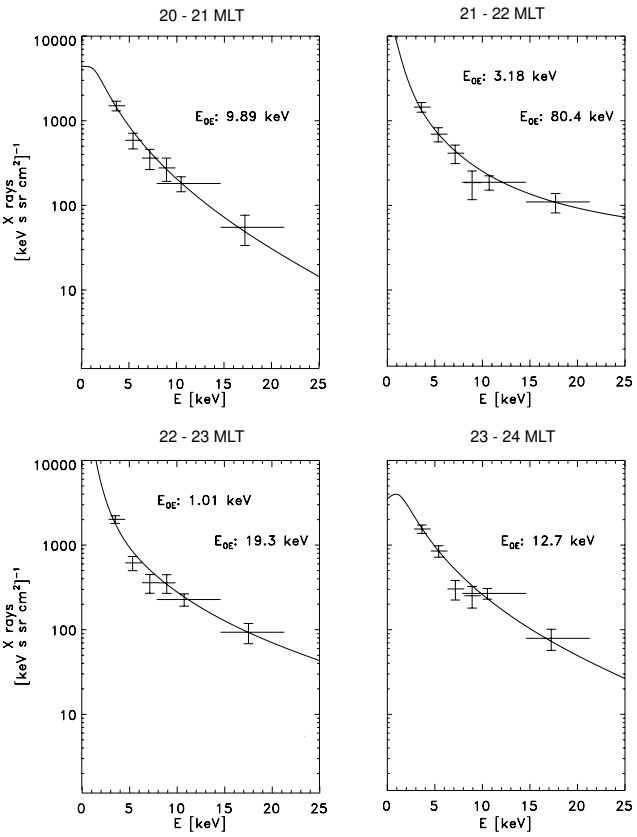

Figure 1. Average X-ray spectra 20 - 24 MLT within 64° and 70° CGM latitude at 0300-0305 UT on July 31, 1997. The width of the energy bands and the statistical errors are shown by horizontal and vertical lines. The smoothed line shows the best fit of X-ray production from either a single or a double exponential electron spectrum. The *e*-folding values of the parent electron spectra are shown in each plot.

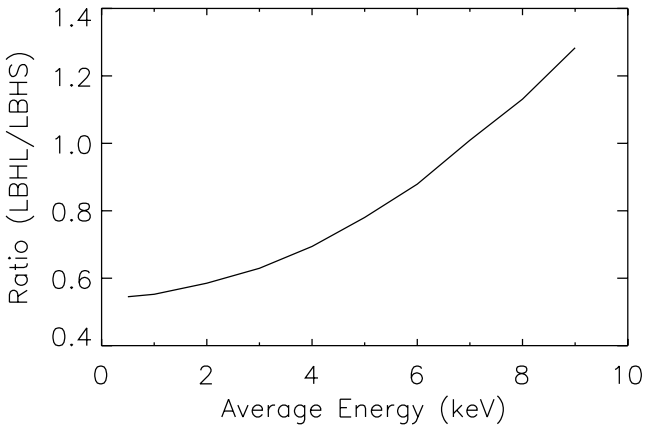

Figure 2. The modeled ratio of LBHL/LBHS as a function of average electron energy. Gaussian energy distributions peaking at E_{AV}, with a full width half maximum of 0.5[ln 2]$^{1/2}E_{AV}$ have been used to represent the precipitating electrons.

will be strongly affected by absorption on their way out of the atmosphere. Thus the intensities of LBHL and LBHS depend differently on the incoming electron average energy and the ratio of LBHL/LBHS intensities can be used to derive the average electron energy [*Germany et al.*, 1997, 1998a, 1998b]. Figure 2 shows the modeled ratio of LBHL/LBHS as a function of average electron energy (E_{AV}). To represent the precipitating electrons, we have used Gaussian energy distributions peaking at E_{AV}, with a full width half maximum of 0.5[ln 2]$^{1/2}E_{AV}$. The electron energy flux between 0.1 and 50 keV can then be calculated from the LBHL intensity using the response curve shown by *Germany et al.* [1998b] in their Figure 2. As earlier studies [*Germany et al.*, 1997, 1998a, 1998b] used an average value to convert from UV emissions to electron flux, this represents a slightly more accurate procedure. Knowing the energy flux and the average energy, we present the electron spectrum either as an exponential or a Maxwellian, depending on which one that gives the smoothest transition to the spectrum derived from the X rays. It should be noted that although the energy flux can be calculated from 100 eV to 50 keV, the effective range of the average energy determination is above 1 keV because electrons softer than this deposit their energy at too high an altitude to be affected by O_2 absorption. Thus for average energies below 1 keV the ratio of LBHL to LBHS flattens out, as can be seen from Figure 2. The sensitivity of the UVI instrument is ∼10-100 R. Using 50 R as a lower limit, model runs using electron fluxes of 1 erg cm^{-2} show that emissions produced by electron energies between 100 eV and 50 keV will be detected in the LBHL wavelength region. We therefore use 0.1 - 50 keV as the valid energy range for the electron spectra derived from the UV emissions. Combined with the electron spectra derived from the X rays, we obtain the electron energy spectra from 100 eV to 100 keV. The exposure time for the LBHL images shown in Plate 1a is 36.8 s. As both LBHL and LBHS are needed to derive electron parameters, the time resolution becomes 1 min 51 s, due to the cycling of filters. When combined with the PIXIE measurements, we therefore use the average of those UVI image time frames (of 1 min 51 s) whose center time falls within the 5-min duration of the X-ray measurements. For the UVI measurements the magnetic apex coordinate system is used, and for PIXIE the CGM coordinates are used. They agree to within less than 0.2°in latitude (∼20 km), which is small compared to the spatial resolution used in this study.

3. Discussion

In Figures 3 and 4 we show six electron spectra derived using the method described above. The high-energy part of the spectra is derived from the PIXIE measurements and shows either a single or double exponential spectrum. The low-energy part of the spectra is a two-parameter spectrum derived from UVI presented as an exponential or as a Maxwellian, depending on what makes the best match to the shape and the magnitude of the spectrum derived from PIXIE. The valid energy ranges for the spectra derived from UVI and PIXIE are determined from what produces 90% of the observed UV emissions and X rays, that is, the energy limits vary with the hardness of the spectra. However, we do not allow the valid energy ranges for the two components of the derived electron spectra to exceed the absolute valid energy ranges determined by the sensitivity of the two instruments, which are electron energies from 0.1 to 50 keV for UVI and above 3 keV for PIXIE. The degree of continuity seen in the combined derived spectra is representative for the entire data set of derived spectra. Also shown are the spectra from 90 eV to 30 keV measured by the SSJ/4 instrument [*Hardy et al.*, 1984] on board the DMSP spacecraft as they passed through the ∼700-km box during the 5 min accumulation time of the PIXIE images. The DMSP measurements are from the Southern Hemisphere, and the trajectories are therefore traced along the magnetic field using CGM coordinates to get the conjugate magnetic trajectories in the Northern Hemisphere. As all the passes are through boxes centered equatorward of 66° CGM latitude, the size of the boxes should be close to the spatial resolution

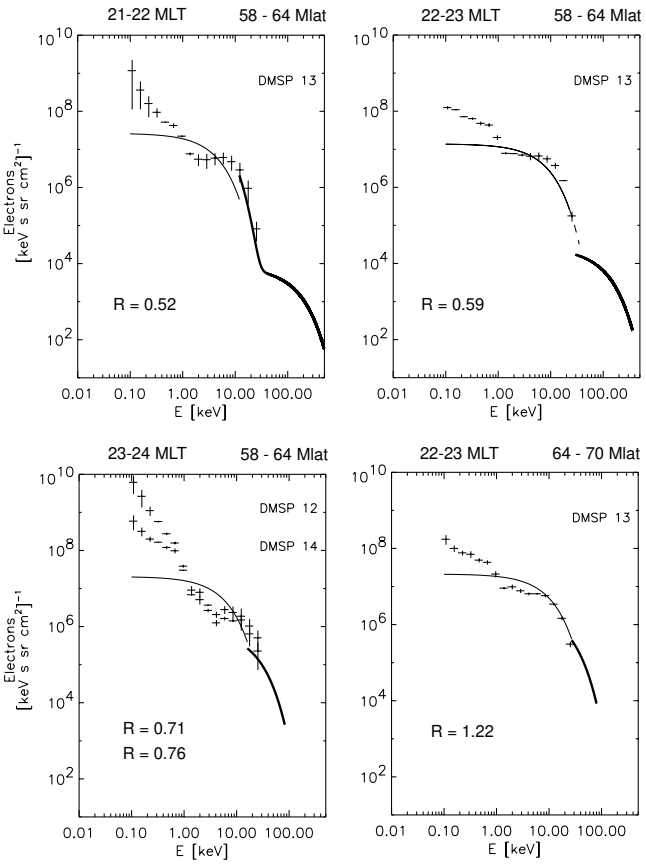

Figure 3. Derived and measured electron spectra at 0315-0320 UT on July 31, 1997. Solid curves are electron spectra derived from UVI and PIXIE. Low-energy part of the spectrum is derived from UVI, and the high-energy part is derived from PIXIE. Pluses are electron spectra measured by the DMSP spacecraft from the Southern Hemisphere traced to the Northern Hemisphere along magnetic field lines using CGM coordinates. R is the ratio of derived energy flux to measured energy flux (by DMSP 12, 13, and 14) in the energy range from 90 eV to 30 keV.

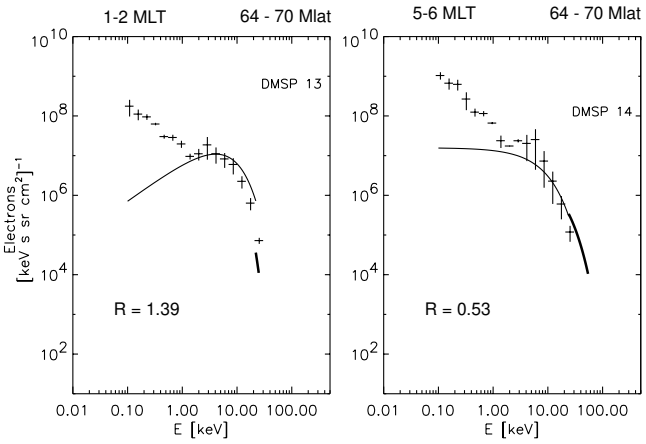

Figure 4. Same as Figure 3 from 0230-0235 UT on July 9, 1997.

of the PIXIE data. We only use the DMSP measurements above 90 eV as the spectrum below this energy also includes photoelectrons from the spacecraft. As an estimate of the expected variations, we use the average spectrum and the maximum spectrum from the DMSP measurements within the various ∼700-km boxes. Maximum spectrum is defined as the spectrum along the satellites trajectory within the ∼700-km box with the highest energy flux between 1 and 30 keV. The motivation for doing this is that the loss cone at the 800 km altitude of DMSP is within ∼50° pitch angle at these latitudes and the SSJ/4 only provides measurements within pitch angles $< 15°$. Hence the derived electron spectra would only be comparable to the average spectrum given that the electron distribution is isotropic in the loss cone. Any presence of anisotropic electron fluxes within the loss cone would produce more UV emission and X rays than the average measured spectrum. Therefore the derived electron spectra should be somewhere between the average and the maximum spectrum measured by DMSP [*Østgaard et al.*, 2000]. Keeping in mind that in situ measurements along the satellite trajectory only cover a small part of the ∼700-km box used to derive the average electron spectra from the imagers measurements, we see that the shape and magnitude of the spectra are in fairly good agreement above ∼1 keV. Below ∼1 keV the DMSP measurements show a low-energy component that is not captured in the derived electron spectra from UVI. For the three time frames we have 16 passes through different ∼700-km boxes where the DMSP measurements and the electron spectra from UVI and PIXIE can be compared. The average ratio of energy flux between 90 eV and 30

keV calculated from UVI and PIXIE and measured by DMSP for the 16 passes is 1.03 ±0.6, which indicates that the energy flux is fairly well extracted from the UV and X-ray measurements. For the DMSP spectra from the 16 passes the average ratio of energy flux between 90 eV and 1 keV (low-energy portion) and energy flux between 90 eV and 30 keV (total) is 0.16±0.14, indicating that the energy contribution from electrons below 1 keV is relatively small, although the log-log scale used in Figures 3 and 4 tends to exaggerate the discrepancies below 1 keV. As the technique we have used to derive the low-energy part of the electron spectrum from UV emissions only provides a two-parameter representation of the electron spectrum, this implies that we get a slight underestimate (overestimate) below (above) 1 keV. Furthermore, we think that the discrepancy below 1 keV to a large extent stems from the limitation in the deriving technique by only providing two parameters to represent the electron spectra below 10 keV when the true electron spectrum cannot be represented by only two parameters in that energy range. All the DMSP spectra in Figures 3 and 4 show a two-component shape that requires more than two parameters to make a more precise functional fit.

When comparing electron measurements along a trajectory that only covers a very small part of the area used for the derived electron spectra, one should not expect a one-to-one correlation. Even by averaging the measured spectra along the trajectory spatially structured precipitation can still lead to large discrepancies. The transformation of the measurements from the Southern Hemisphere to the Northern Hemisphere introduces uncertainties as well. The large standard deviation of the average ratio of measured and derived electron flux reflects this, although the average ratio itself is fairly good.

In Plate 2 we show the electron energy flux derived from UVI and PIXIE on a global scale. For this display we have oversampled spatially by a factor of 3 and provided a boxcar averaging. The total energy fluxes from 100 eV to 100 keV, as well as the low- and high-energy component of the energy flux are shown. The energy flux should be the most accurate derived parameter from the imagers and the deriving technique from the UV emissions seems to compensate for the discrepancy below 1 keV by slightly overestimating the fluxes above 1 keV. We therefore believe that the maps of energy flux below and above 10 keV give a fairly precise estimate of the energy deposition in the two energy ranges. The global maps in Plate 2 show that the energy deposition of different energies occur in different regions of space. This implies that energy deposition occurs nonuniformly with some regions obtaining more energy fluxes from lower energy electron precipitation, while in other regions, the enhancement is primarily due to the high-energy precipitation. For the two time frames shown here it can be seen that the energy deposition in the evening sector is mainly due to electrons below 10 keV, while the energy deposition in the premidnight and morning sector is provided by more energetic electrons. Such features enable one to see how the magnetosphere accelerates and precipitates electrons and how the coupling is achieved. The more energetic electrons penetrate deeper into the atmosphere and can affect the electrodynamics by enhancing the conductivity and thereby affect the ionospheric currents.

4. Summary

We have shown that the combined UV and X-ray emissions can be used to obtain the electron energy flux from 100 eV to 100 keV as well as the shape of the electron spectra from 1 keV to 100 keV. Two independent techniques have been used to derive electron spectral parameters from UVI and PIXIE. The resulting combined spectra are physically reasonable and nearly continuous. The comparison with the DMSP spectra shows that we are able to capture the shape and magnitude of the true electron spectra fairly well above ∼1 keV. Due to the relatively small cross section for bremsstrahlung X-ray production, the best resolution we can achieve, given that we want to monitor the entire auroral oval, is 5 min averages in ∼700-km boxes. The method enables us to present the first global maps of the Northern Hemisphere of electron energy deposition in the energy range from 100 eV to 100 keV into the ionosphere during precipitation events. We have shown that the combination of UV and X-ray cameras on a polar orbiting spacecraft enables a comprehensive monitoring of the global energy deposition from precipitating electrons over the energy range that is important for understanding the MI-coupling physics.

Acknowledgments. This study was supported by the Norwegian Research Council (NFR) and by the National Aeronautic and Space Administration (NASA) under contract NAS5-30372 at the Lockheed-Martin Advanced Technology Center, the University of Washington contract 832213 to the University of Alabama in Huntsville and NASA grant NAG5-6986 to the University of Alabama in Huntsville. We want to thank F. Rich at Space Physics Model Branch at AFRL/VSBP for providing data from the DMSP SSJ/4 particle detectors.

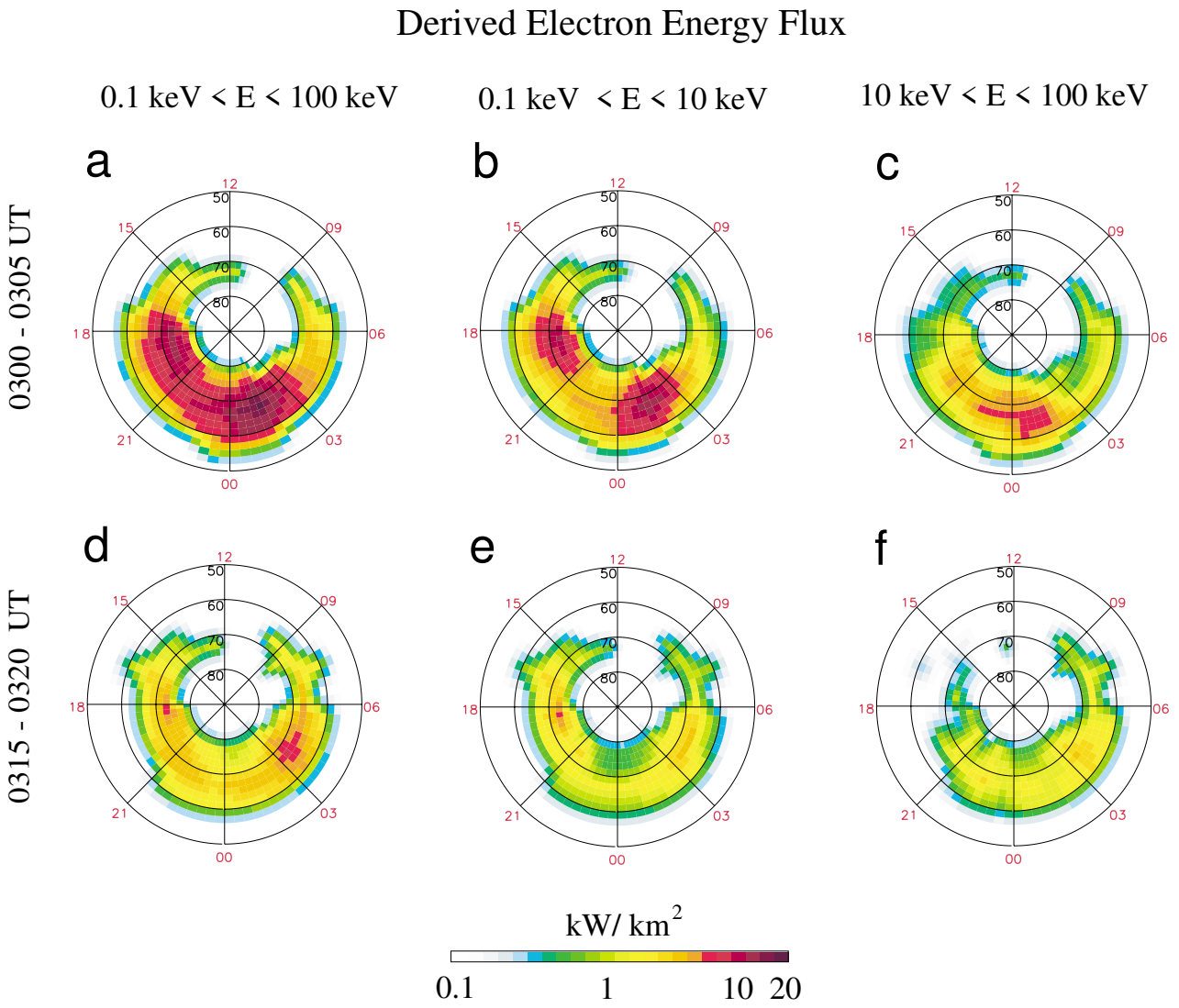

Plate 2. Global maps of derived electron energy flux based on the combined measurements from UVI and PIXIE. (a, d) The total energy flux (0.1 - 100 keV). (b, e) The low-energy component of the energy flux (0.1 - 10 keV). (c, f) The high-energy component of the energy flux (10 - 100 keV).

Janet G. Luhmann thanks James F. Carbary and Michael G. Henderson for their assistance in evaluating this paper.

References

Acuña, M. H., K. W. Ogilivie, D. N. Baker, S. A. Curtis, D. H. Fairfield, and W. H. Mish, The global geospace science program and its investigations, *Space Sci. Rev.*, *71*, 5, 1995.

Anderson, P. C., D. L. Chenette, D. L. McKenzie, J. M. Quinn, M. Grande, and M. Carter, Energetic auroral electron distribution derived from global X-ray measurements and comparison with in-situ particle measurements, *Geophys. Res. Lett.*, *25*, 4105, 1998.

Berger, M. J., and S. M. Seltzer, Bremsstrahlung in the atmosphere, *J. Atmos. Terr. Phys.*, *34*, 85, 1972.

Berger, M. J., S. M. Seltzer, and K. Maeda, Energy deposition by auroral electrons in the atmosphere, *J. Atmos. Terr. Phys.*, *32*, 1015, 1970.

Eather, R. H., and S. B. Mende, Airborne observations of auroral precipitation patterns, *J. Geophys. Res.*, *76*, 1746, 1971.

Germany, G. A., G. K. Parks, M. Brittnacher, J. Cumnock, D. Lummerzheim, J. F. Spann, L. Chen, P. G. Richards, and F. J. Rich, Remote determination of auroral energy characteristics during substorm activity, *Geophys. Res. Lett.*, *24*, 995, 1997.

Germany, G. A., G. K. Parks, M. J. Brittnacher, J. F. Spann, J. Cumnock, D. Lummerzheim, F. Rich, and F. G. Richards, Energy characterization of a dynamic auroral event using GGS UVI images, in *Geospace Mass and Energy Flow: Results From the International Solar-Terrestrial Physic Program, Geophys. Monogr. Ser.,* vol. 104, edited by J. L. Horwitz, D. L. Gallagher, and W. K. Peterson, p. 143, AGU, Washington, D. C., 1998a.

Germany, G. A., J. F. Spann, G. K. Parks, M. J. Brittnacher, R. Elsen, L. Chen, D. Lummerzheim, and M. H. Rees, Auroral observations from the POLAR Ultraviolet Imager (UVI), in *Geospace Mass and Energy Flow: Results From the International Solar-Terrestrial Physic Program, Geophys. Monogr. Ser.,* vol. 104, edited by J. L. Horwitz, D. L. Gallagher, and W. K. Peterson, p. 149, AGU, Washington, D. C., 1998b.

Gorney, D. J., Satellite-based remote sensing of aurora, in *Quantitative Modelling of Magnetosphere - Ionosphere Coupling Processes*, edited by Y. Kamide and R. Wolf, p. 197, Kyoto Sangyo Univ., Kyoto, Japan, 1987.

Hardy, D. A., L. K. Schmitt, M. S. Gussenhoven, F. J. Marshall, H. C. Yeh, T. L. Shumaker, A. Hube, and J. Pantazis, Precipitating electron and ion detectors (SSJ/4) for the block 5D/flights 6-10 DMSP satellites: Calibration and data presentation, *Tech. Rep. AFGL-TR-84-0317*, Air Force Geophys. Lab., Hanscom Air Force Base, Mass., 1984.

Imhof, W. L., et al., The Polar Ionospheric X-ray Imaging Experiment (PIXIE), *Space Sci. Rev.*, *71*, 385, 1995.

Kamiyama, H., Flux of bremsstrahlung photons caused by energetic electrons precipitating into the upper atmosphere, *Rep. Ionos. Space Res. Jpn.*, *20*, 374, 1966.

Khosa, P. N., R. R. Rausaria, and K. L. Moza, Spectrum, angular distribution and polarization of auroral hard X rays, *Planet. Space Sci.*, *32*, 31, 1984.

Lorence, L. J., CEPXS/ONELD Version 2.0: A discrete ordinates code package for general one-dimensional coupled electron-photon transport, *IEEE Trans. Nucl. Sci.*, *39*, 1031, 1992.

Luhmann, J. G., and J. B. Blake, Calculations of soft auroral bremsstrahlung and Kα line emission at satellite altitude, *J. Atmos. Terr. Phys.*, *39*, 913, 1977.

Miller, K. L., and R. R. Vondrak, A high-latitude phenomenological model of auroral precipitation and ionospheric effects, *Radio Sci.*, *20*, 431, 1985.

Østgaard, N., J. Bjordal, J. Stadsnes, and E. Thorsen, PIXIE data processing at the University of Bergen, *Tech. Rep. 1999-05*, Univ. of Bergen, Bergen, Norway, 1999.

Østgaard, N., J. Stadsnes, J. Bjordal, R. R. Vondrak, S. A. Cummer, D. Chenette, M. Schulz, and J. Pronko, Cause of the localized maximum of X-ray emission in the morning sector: A comparison with electron measurements, *J. Geophys. Res.*, *105*, 20,869, 2000.

Rees, M. H., Ionization in the Earth's atmosphere by aurorally associated bremsstrahlung X rays, *Planet. Space Sci.*, *12*, 1093, 1964.

Rees, M. H., and D. Luckey, Auroral electron energy derived from ratio of spectroscopic emissions, 1. Model computations, *J. Geophys. Res.*, *79*, 5182, 1974.

Robinson, R. M., and R. R. Vondrak, Validation of techniques for space based remote sensing of auroral precipitation and its ionospheric effect, *Space Sci. Rev.*, *69*, 331, 1994.

Robinson, R. M., G. T. Davidson, R. R. Vondrak, W. E. Francis, and M. Walt, A technique for interpretation of auroral bremsstrahlung X-ray spectra, *Planet. Space Sci.*, *37*, 1053, 1989.

Seltzer, S. M., and M. J. Berger, Bremsstrahlung in the atmosphere at satellite altitudes, *J. Atmos. Terr. Phys.*, *36*, 1283, 1974.

Steele, D. P., and D. J. McEwen, Electron auroral excitation efficiencies and intensity ratios, *J. Geophys. Res.*, *95*, 10,321, 1990.

Strickland, D. J., and D. E. J. Anderson, Dependence of auroral FUV emissions on the incident electron spectrum and neutral atmosphere, *J. Geophys. Res.*, *88*, 8051, 1983.

Torr, M. R., et al., A far ultraviolet imager for the international solar-terrestrial physics mission., *Space Sci. Rev.*, *71*, 329, 1995.

Walt, M., L. L. Newkirk, and W. E. Francis, Bremsstrahlung produced by precipitating electrons, *J. Geophys. Res.*, *84*, 967, 1979.

J. Bjordal and J. Stadsnes, Department of Physics, University of Bergen, N-5007, Bergen, Norway.

D. L. Chenette, Solar and Astrophysics Laboratory Organization L9-41, Building 252, Lockheed Martin

Advanced Technology Center 3251 Hanover Street, Palo Alto, CA, 94304, USA.

S. A. Cummer, Electrical and Computer Engineering Department, Duke University, Durham, NC 27708, USA.

G. A. Germany, The Center for Space Plasma, Aeronomy, and Astrophysics Research, University of Alabama in Huntsville, Huntsville, AL 35899, USA.

N. Østgaard and R. R. Vondrak, Laboratory for Extraterrestrial Physics, Code 690, Building 2, NASA GSFC, Greenbelt, MD 20771, USA. (ostgaard@lepvax.gsfc.nasa.gov)

G. K. Parks, Geophysics Program, University of Washington, Seattle, WA 98195, USA.

J. G. Pronko, Physics Department, University of Nevada, Reno, NV 89507, USA.

January 30, 2001; revised April 16, 2001; accepted April 17, 2001.

This preprint was prepared with AGU's LaTeX macros v4, with the extension package 'AGU^{++}' by P. W. Daly, version 1.6b from 1999/08/19.